Journal of Engg. Research Vol. 7 No. (1) March 2019 pp. 1-11

Novel planar lowpass filter using microstrip rectangular patch and high-impedance cells for wireless communication systems

Abbas Rezaei* and Leila Noori**

*Department of Electrical Engineering, Kermanshah University of Technology, Kermanshah, Iran
**Young Researchers and Elite Club, Kermanshah Branch, Islamic Azad University, Kermanshah, Iran
a.rezaee@kut.ac.ir, unrezaei@yahoo.com, leila_noori62@yahoo.com
** Corresponding Author (Email: Leila_noori62@yahoo.com

ABSTRACT

This paper presents a novel microstrip lowpass filter. The proposed filter consists of two high impedance cells, which are integrated by a stub loaded transmission line. A rectangular stub is utilized to reduce the overall circuit size so that it has a compact size of 0.0135 λ_g^2 where λg is the guided wavelength calculated at 2.5 GHz. In comparison to the previous works, a good figure of merit (FOM) is obtained, which indicates that this filter is designed correctly. An approximated LC circuit is introduced to analyse the configuration of the proposed structure. Based on the transmission line theory, the lumped elements are calculated. Then, the LC model is simulated where the obtained results are approximately similar to the EM simulator results. In order to verify the design methodology, the proposed filter is fabricated and measured. There is a good agreement between the simulation and measurement results.

Keywords: Microstrip; Filter; Low pass; Compact; Wireless communication.

INTRODUCTION

Microstrip devices such as single-band and multi-band bandpass filters (Ghazali et al., 2018, 2017; Karpuz et al., 2016), couplers (Sohn et al., 2016; Wang et al., 2017), diplexers (Li and Zhang, 2017; Rezaei et al., 2017), multiplexers (Deng et al., 2015), etc. are widely demanded by RF/Microwave communication systems. These devices have filtering frequency responses. Accordingly, a well-designed microstrip filter can be an initial design idea for obtaining the other microstrip devices. Planar microstrip lowpass filters (LPFs) are essential devices in modern wireless communication systems. They separate lower frequency spectrum for using in the developed telecommunication systems. Therefore, various types of LPFs have been proposed to achieve planar architecture factor (AF), small normalized circuit size (NCS), high sharpness (ξ), high relative stopband bandwidth (RSB), and good suppression factor (SF). The effect of these parameters is summarized in figure of merit (FOM). However, most of the previous works (Majidifar, 2016; Hayati and lotfi, 2010; Verma et al., 2013; Chen et al., 2007; Yang et al., 2012; Karthikeyan and Kshetrimayum, 2015; Mirzaee and Virdee, 2013; Sariri et al., 2013; Li and Li, 2008; Verma and Kumar, 2011) could not reach a good FOM. Moreover, a number of the published references only optimized the other previous structures. This means that they could not propose a novel structure with good performance. For example, the proposed structure in Hayati and lotfi (2010) is optimized in Majidifar (2016) so that in both of them the same stubs are utilized. In addition, the proposed LPFs in Verma and Kumar (2013) and Chen et al. (2007) are similar so that a major part of their layouts consists of the same step impedance structures. We can see another structural similarity in Yang et al. (2012) and Karthikeyan and Kshetrimayum (2015), where they employ the same microstrip spiral structures. However, designers in Karthikeyan and Kshetrimayum (2015) and Majidifar (2016) could reduce the circuit size. In Mirzaee and Virdee (2013), new stub loaded lowpass filter has been realized with low insertion loss. In Sariri et al. (2013), angular and T-shape cells have been utilized to achieve wide stopband. In Li and Li (2008), a quasi-elliptic lowpass filter has been designed using two interdigital units to attenuate the harmonics from 2.8 GHz to 9.3 GHz. Symmetric rectangular coupled capacitors have

been utilized to obtain a LPF in Verma and Kumar (2011). To achieve a high FOM, a novel LPF with large size has been introduced using coupled-line resonator (Velidi and Sanyal, 2011). The LPFs designed in Sariri et al. (2013); Li and Li (2008); Verma and Kumar (2011); Velidi and Sanyal (2011) occupy large implementation area.

In this paper, a compact LPF is designed using a novel structure. Its cut-off frequency is at 2.5 GHz so that the proposed filter can be used for wireless applications. To reduce the filter size a patch stub and high impedance units are used. The proposed filter has a good figure of merit, which is obtained based on a novel structure where several of reported LPFs only optimized the previous structures. The designing method is based on analysing the proposed LPF using its approximated LC model so that the values of lumped elements are calculated based on the transmission line theory. The approximated LC circuit is simulated and the obtained results are similar to EM simulator. A mathematical method is presented to obtain a perfect impedance matching, which is applied to improve the insertion loss.

Analysis of Filter Structure

Most of the designed lowpass filters include a transmission line loaded by various types of cells while the coupled lines are used to create bandpass channels. The patch cells are able to save the size while they can properly move cut-off frequency to the left. Furthermore, by tuning the widths of a high impedance section a high degree of freedom can be obtained to control the filter performance. Accordingly, the use of rectangular patch and high impedance sections is preferred. The microstrip cells, which are utilized to design our lowpass filter, are presented in Figs.1(a), 1(b) and (1c). The equivalent LC circuits of all parts are also depicted, where the open ends are replaced by capacitors. The LC model of high impedance cell presented in Figure 1a is obtained using the proposed LC circuit in Hong and Lancaster (2001).

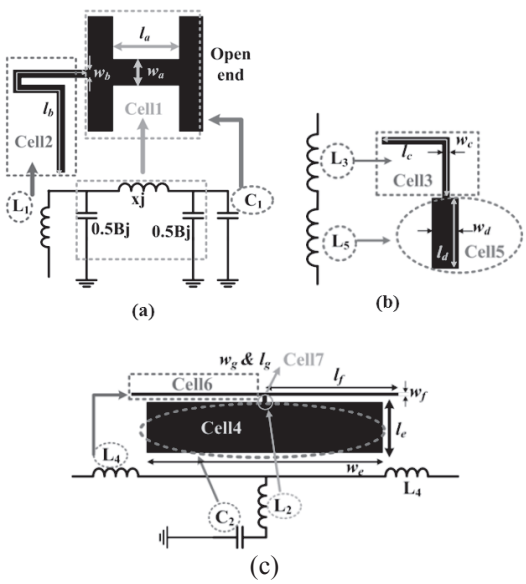

Fig. 1. (a) High impedance cell connected to a microstrip line, (b) step impedance cell, and (c) stub-loaded microstrip line.

Since the effects of bents and steps in widths are significant at the frequencies higher than 10 GHz, we ignored them. The microstrip cell in Figure 1(c) is utilized as feed structure and the unit in Figure 1(b) integrates the other microstrip parts. The LC equivalent model of high impedance section can be defined as follows (Wadell, Brian C, 1991):

$$x = Z_c \sin(\frac{2\pi}{\lambda_g} l); \quad for \ l \langle \frac{\lambda_g}{8} \Rightarrow x \approx Z_c \frac{2\pi}{\lambda_g} l \tag{1.a}$$

$$0.5B = \frac{1}{Z_c} \tan(\frac{\pi l}{\lambda g}); for \ l \langle \frac{\lambda_g}{8} \Rightarrow 0.5B \approx \frac{\pi l}{Z_c \lambda_g} \tag{1.b}$$

where

$$for\ \frac{w}{h} \geq 1: \quad \begin{cases} Zc = \dfrac{120\pi}{[\frac{w}{h} + 1.393 + 0.677\ln(1.44 + \frac{w}{h})]\sqrt{\varepsilon_{re}}} \\ \varepsilon_{re} = \dfrac{\varepsilon_r + 1}{2} + \dfrac{\varepsilon_r - 1}{2\sqrt{1 + 12\frac{h}{w}}} \end{cases} \tag{1.c}$$

$$for\ \frac{w}{h} \leq 1: \quad \begin{cases} Zc = \dfrac{120\pi}{\sqrt{\varepsilon_{re}}}\ln(\frac{8h}{w} + 0.25\frac{w}{h}) \\ \varepsilon_{re} = \dfrac{\varepsilon_r + 1}{2} + [\dfrac{1}{\sqrt{1 + \frac{12h}{w}}} + 0.04(1 - \frac{w}{h})^2]\dfrac{\varepsilon_r - 1}{2} \end{cases} \tag{1.d}$$

$$\lambda_g\,(mm) = \frac{300}{f\,(GHz)\sqrt{\varepsilon_{re}}} \tag{1.e}$$

In Equation (1), *l, w, h, f, Z_c* and ε_{re}, are the physical length presented in Figure1(a), width, thickness of substrate, cut-off frequency for LPF, characteristic impedance, and effective dielectric constant, respectively.

Based on transmission line theory, the values of other lumped elements presented in Figs.1(a), 1(b) and 1(c) can be calculated using the input impedance of a transmission line (Z_{ink}). A microstrip cell with the physical length lk has an input impedance of Z_{ink} that can be calculated for inductive and capacitive modes at a frequency of "f" as follows (Wadell, Brian C, 1991):

$$Inductive\ \text{mode}: \quad Z_{ink} = jZ_c \tan(\frac{2\pi l_k}{\lambda g}) \tag{2.a}$$

$$\text{Capacitive mode}: \ Z_{ink} = \frac{-jZ_c}{\tan(\frac{2\pi l_k}{\lambda g})} \tag{2.b}$$

According to the transmission line theory, for an open-end stub, Z_{ink} should be calculated using Equation (2.b) (Wadell, Brian C, 1991). To obtain the lumped elements, we need the physical dimensions, ε_{re}, Z_c and Z_{ink} as listed in Table 1. By selecting ε_r = 2.2 and h = 0.7874 mm, the parameters Z_c, λg and ε_{re} will have different values for certain amount of widths, which are calculated according to Equation (1) (see Table 1). According to the physical dimensions and calculated data in Table 1, the values of lumped elements are obtained and listed in Table 2 .

Table 1. Physical dimensions of the microstrip cells, basic data and calculated lumped elements.

Specification	Physical lengths	Physical widths	ε_{re}	Z_c (Ω)	λ_g at 2.5 GHz	Z_{ink} (Ω)
Cell1	l_a=1.5 mm	w_a=1 mm	1.785	84.49	89.8	---
Cell2	l_b=4.3mm	w_b=0.2mm	1.699	158.86	92	48j
Cell3	l_c=3mm	w_c=0.1mm	1.679	191.82	92.6	39.6j
Cell4	l_e=12mm	w_e=2mm	1.851	56.92	88	-49.3j
Cell5	l_d=1.5 mm	w_d=0.3mm	1.768	139.71	90.2	14.6j
Cell6	l_f=4.7mm	w_f=0.1mm	1.679	191.82	92.6	63.3j
Cell7	l_g=0.2mm	w_g=0.2mm	1.699	158.86	92	2.17j

Table 2. Calculated lumped elements.

Specification	Modes	Lumped Elements
Cell1	Capacitive/Inductive	---
Cell2	Inductive	L_1=3.05 nH
Cell3	Inductive	L_3=2.52 nH
Cell4	Capacitive	C_2=0.134 pF
Cell5	Inductive	L_5=0.92 nH
Cell6	Inductive	L_4=0.93 nH
Cell7	Inductive	L_2=0.14 nH

Since our aim is a cut-off frequency at 2.5 GHz, λg is calculated at this frequency. According to Equations (1.a), (1.b) and Table 1, B and x (see Figure 1(a)) are -0.00124 and 8.85, respectively. Using these values, the inductors and capacitors of cell1 are 0.56 nH and 0.102 pF, respectively. Z_{ink} for inductive and capacitive modes is calculated using Equation (2) and the obtained data are shown in Table 1. In addition, using Equation (2) the open-end capacitor is calculated as C_1=0.7 pF. In Tables 1 and 2, each row is related to a cell outlined in Figure 1. Using the microstrip cells depicted in Figure 1(a), the proposed LPF is designed as shown in Figure 2. Its corresponding dimensions are listed in Table 3. It consists of two high impedance resonators, which are connected by a stub loaded unit. This stub is a rectangular patch. It can shift the cut-off frequency to the left without significant increase in size.

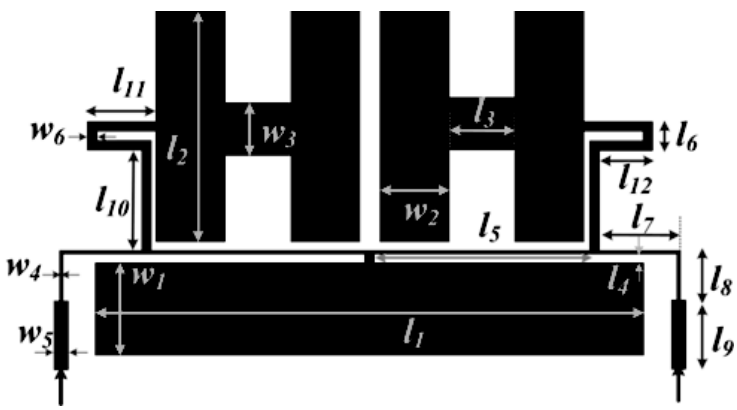

Fig. 2. Proposed lowpass filter.

Table 3. Dimensions of the proposed lowpass filter.

Parameters	l_1	l_2	l_3	l_4	l_5	l_6	l_7	l_8	l_9
Values (mm)	12	5	1.5	0.2	4.7	0.6	1.8	1.2	1.5
Parameters	l_{10}	l_{11}	l_{12}	w_1	w_2	w_3	w_4	w_5	w_6
Values (mm)	2.2	1.5	1.2	2	1.5	1	0.1	0.3	0.2

The approximated LC circuit of the proposed structure is demonstrated in Figure 3(a), where we ignore the effects of bents and step-in-widths. Usually, the effects of bents and step-in-widths are only significant at the frequencies higher than 10 GHz. As shown in Figure 3(a), a high impedance section is replaced by a π-structure including two capacitors of 0.5Bj and an inductor of xj. The capacitors C_1 and C_2 present the open end of high impedance and rectangular patch

cells. The physical lengths l_6, l_{10}, l_{11} and l_{12} are modeled by an inductor of L_1, while the inductor L_3 depicts the effect of physical lengths l_7 and l_8. The inductors L_4 and L_5 are related to the thin microstrip cells with physical lengths l_5 and l_9, respectively. The small stub connected to the rectangular patch cell is presented by L_2 that has a relatively low value. These inductors and capacitors are calculated based on Table 2. Figure 3(b) shows an equivalent model of Figure 3(a), where Z_1, Z_2 and Z_3 are the defined impedances in the LC circuit. The equivalent circuit presented in Figure 3(b) is employed to make the calculation of transmission matrix easier. As illustrated in Figure 3(b), impedance Z_1 is seen from the inductor L_1 to the open-end capacitor while $Z_2 = j\omega (L_3+L_5)$ and $Z_3 = j\omega L_2 + 1/(j\omega C_2)$ for an angular resonance frequency of ω. Due to having a very small L_2, it can be ignored in calculating Z_3. This LC circuit is simulated for three cases so that three results are obtained. The simulation results of the LC model are presented in Figures 3(c) and 3(d). In two cases we entered the effect of step between cell4 and cell7 by adding a parallel capacitor C_e between L_2 and C_2 for C_e=0.4 pF and C_e=1.2 pF. In the third case, we removed this capacitor. As shown in Figures 3(c) and 3(d), the LC circuit has a lowpass frequency response with a cut-off frequency near 2.5 GHz. However, due to having an approximated LC circuit, the simulation results obtained from the LC model and layout configuration are a little different, because in higher frequencies the effects of bents and steps, which we ignored in our approximated LC model, are more significant. By increasing capacitor C_e, the return loss can be improved (see Figure 3(d)). However, removing this capacitor improves the stopband properties. By using Figure 3(b), the transmission matrix of the proposed filter can be written as follows:

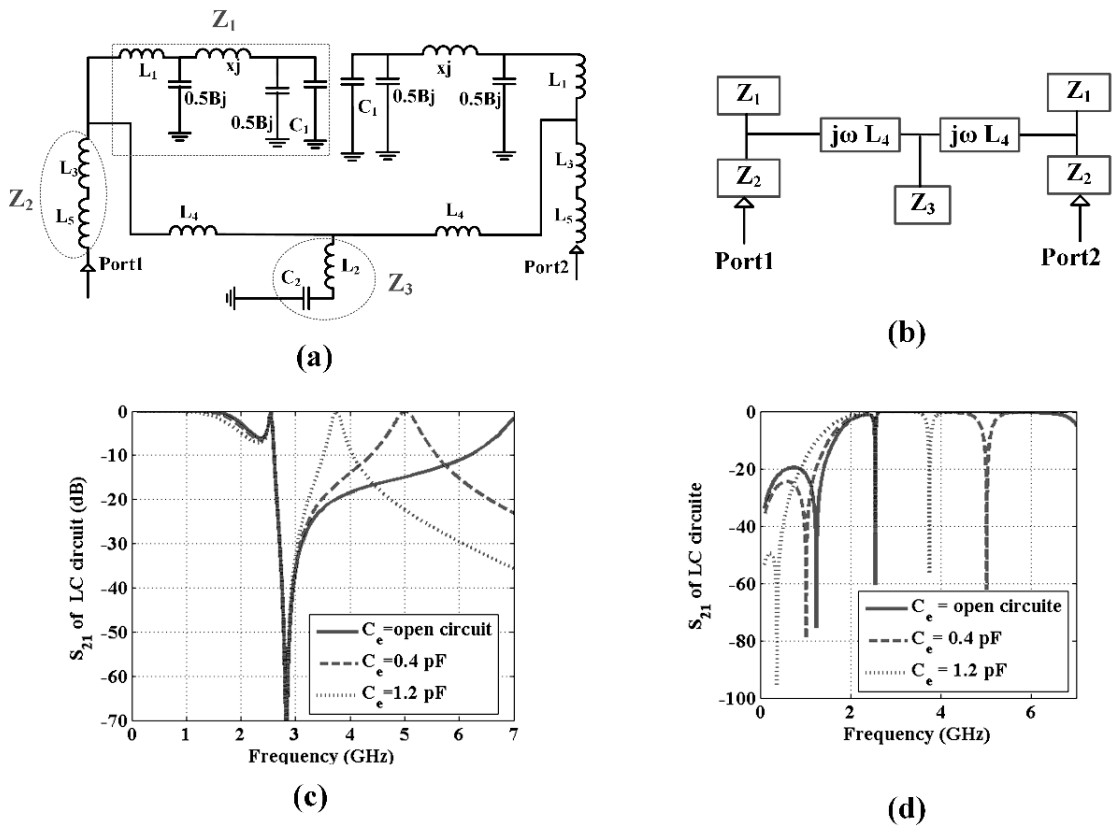

Fig. 3. (a) LC model of proposed LPF, (b) equivalent model of the proposed LC circuit, (c) simulated S_{21} for LC model, and (d) simulated S_{11} for LC model.

$$T=\begin{bmatrix}1 & Z_2\\ 0 & 1\end{bmatrix}\times\begin{bmatrix}1 & 0\\ \frac{1}{Z_1} & 1\end{bmatrix}\times\begin{bmatrix}1 & j\omega L_4\\ 0 & 1\end{bmatrix}\times\begin{bmatrix}1 & 0\\ \frac{1}{Z_3} & 1\end{bmatrix}\times\begin{bmatrix}1 & j\omega L_4\\ 0 & 1\end{bmatrix}\times\begin{bmatrix}1 & 0\\ \frac{1}{Z_1} & 1\end{bmatrix}\times\begin{bmatrix}1 & Z_2\\ 0 & 1\end{bmatrix}=\begin{bmatrix}A & B\\ C & D\end{bmatrix}$$

where:

$$A=[(1+\frac{Z_2}{Z_1})(1+\frac{j\omega L_4}{Z_3})+\frac{Z_2}{Z_3}](1+\frac{j\omega L_4}{Z_1})+\frac{(1+\frac{Z_2}{Z_1})(j\omega L_4)+Z_2}{Z_1}$$

$$B=[(1+\frac{Z_2}{Z_1})(1+\frac{j\omega L_4}{Z_3})+\frac{Z_2}{Z_3}]\times[j\omega L_4+Z_2(1+\frac{j\omega L_4}{Z_1})]+(1+\frac{Z_2}{Z_1})[(1+\frac{Z_2}{Z_1})(j\omega L_4)+Z_2] \quad (3)$$

$$C=[\frac{1}{Z_1}(1+\frac{j\omega L_4}{Z_3})+\frac{1}{Z_3}](1+\frac{j\omega L_4}{Z_1})+\frac{1}{Z_1}(1+\frac{j\omega L_4}{Z_1})$$

$$D=[\frac{1}{Z_1}(1+\frac{j\omega L_4}{Z_3})+\frac{1}{Z_3}][j\omega L_4+Z_2(1+\frac{j\omega L_4}{Z_1})]+[1+\frac{j\omega L_4}{Z_1}](1+\frac{Z_2}{Z_1})$$

The perfect input impedance matching can be obtained when the reflection coefficient (Γ) is zero. Employing the T matrix, the condition of perfect input impedance matching can be obtained as follows:

$$\Gamma=\frac{A+B-C-D}{A+B+C+D}=0 \quad (4)$$

By substituting Equation (3) into Equation (4), the following result can be obtained:

$$\omega^2\left\{\frac{{L_4}^2}{Z_3}(\frac{1+Z_1}{{Z_1}^3}-1-\frac{2Z_2}{Z_1}-\frac{{Z_2}^2}{{Z_1}^2}\right\}+\omega\left\{jL_4(2+\frac{2{Z_2}^2-2}{Z_3Z_1}+\frac{2Z_2}{Z_3}+\frac{4Z_2}{Z_1}+\frac{2{Z_2}^2-1}{{Z_1}^2}-\frac{2}{{Z_1}^2Z_3}-\frac{1}{{Z_1}^3})\right\}-$$
$$\left\{\frac{1}{Z_1}+\frac{1}{Z_3}+\frac{1}{{Z_1}^2}+\frac{1}{Z_1Z_3}-2Z_2-\frac{2{Z_2}^2}{Z_1}-\frac{{Z_2}^2}{Z_3}\right\}=0$$

where:

(5)

$$\begin{cases}L_4=12.3\times10^{-9}\,H\\ Z_2=j\,\omega(L_3+L_5)=10.7\times10^{-9}\,j\,\omega\\ Z_3\approx\dfrac{1}{j\,\omega C_2}\Rightarrow\dfrac{1}{Z_3}\approx0.34\times10^{-9}\,j\,\omega\Rightarrow-\dfrac{\omega^2{L_4}^2}{Z_3}+2\,j\,\omega\,L_4(1+\dfrac{Z_2}{Z_3})-\dfrac{1}{Z_3}-2Z_2-\dfrac{{Z_2}^2}{Z_3}=0\Rightarrow\omega\approx2.9\times10^4\,Hz\\ Z_1:High\ impedance\ part\Rightarrow\dfrac{1}{Z_1}\approx0\end{cases}$$

Our aim is to obtain the perfect matching in low frequencies. Hence, in Equation (5) ω is a low angular frequency which verifies the perfect matching at low frequencies. The LC model helps to optimize the filter. Since these results are obtained from an approximated circuit, they are not exactly matched with the EM simulator results. However, they are similar to each other considerably. The simulation results of LC model verify the calculated data and proposed geometrical structure. The EM simulator results can be changed as a function of filter dimensions. However, changing some parameters has a significant impact on the filter performance. S_{21} and S_{11} are depicted as a function of l_1, l_{10}, l_9 and w_1 in Figures 4(a), 4(b), 4(c), and 4(d), respectively. As presented in Figures 4(a) and 4(d), by tuning the stub with

physical length l_1 and w_1 we can control the level of harmonic and its position. Figure 4(b) shows the effect of l_{10} on the cut-off frequency. Moreover, the tapped line dimension has an important effect on the return loss (see Figure 4(c)). From Figure 4(a) it is clear that increasing the length l_1 shifts the harmonic to the right while the cut-off frequency almost remains fixed. However, increasing the physical length l_{10} increases harmonic level significantly (see Figure 4(b)). Unlike the previous case, increasing l_{10} shifts the cut-off frequency to the left. As presented in Figure 4(c), changing the length l9 has no effect on harmonics but decreasing this length increases the return loss. The important issue is the bandwidth increment, which can be obtained by increasing the physical length l9. Similar to the effects of l_1 and l_{10}, tuning the width w_1 improves the harmonics so that reducing w_1 shifts the harmonics to the right. On the other hand, a relatively large value of w_1 can decrease the harmonics level.

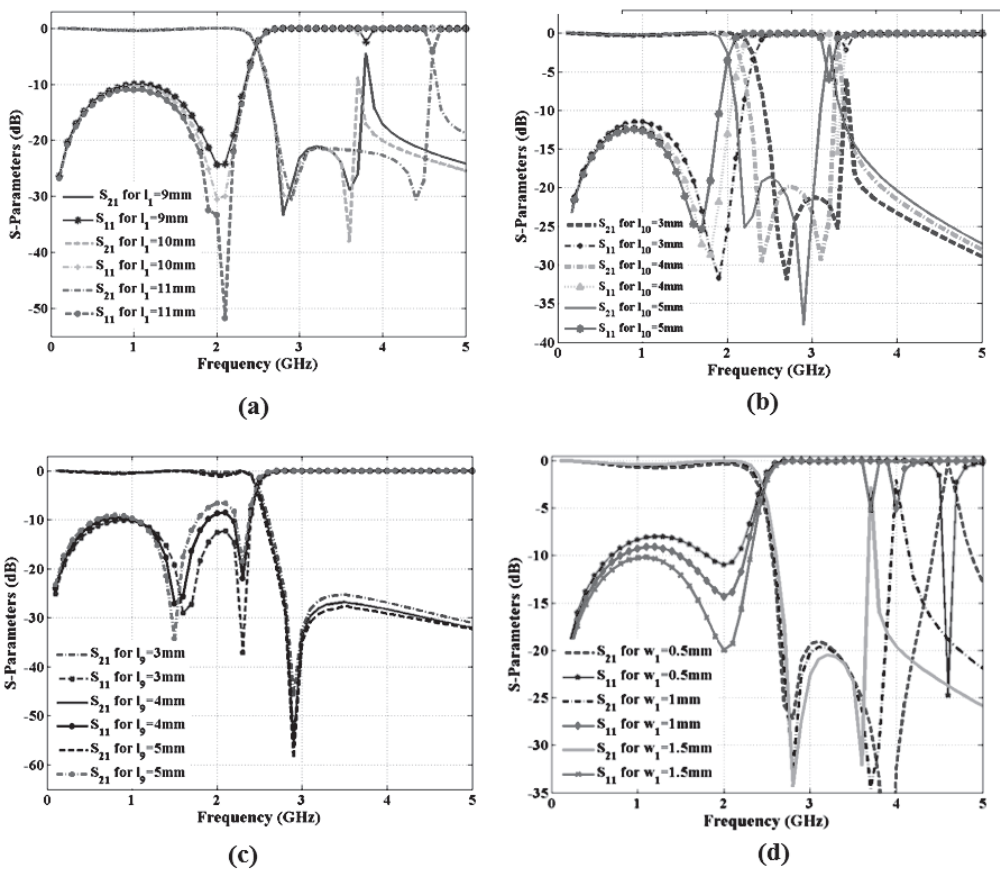

Fig. 4. Simulated S21 and S11 as a function of (a) l1, (b) l10, (c) l9, (d) w1.

The current density distribution of the filter at 1, 2.5, 2.9 and 4.9 GHz is demonstrated in Figure 5. It is clear that the maximum current density is 638.98 A/m, which is obtained at 2.5 GHz. Most of the current density is in the cells with narrow widths such as the stubs with the physical lengths l_5, l_7, l_8 and l_9. As depicted in Figure 5, at 1GHz the maximum current density distribution is aggregated at the rectangular patch cell. Since frequency 1 GHz is before the cut-off frequency, the passband properties such as insertion and return losses can be controlled by adjusting the rectangular cell dimensions. At the cut-off frequency (2.5 GHz), the maximum current density is distributed at the high impedance sections and thin microstrip lines. Accordingly, these cells have more effects on the position of cut-off frequency and selectivity. One of them is the physical length l_9 that we presented its effect on the cut-off frequency and bandwidth. Similarly, the current density distributions at 2.9 GHz and 4.9 GHz can help optimize the out-of-band properties.

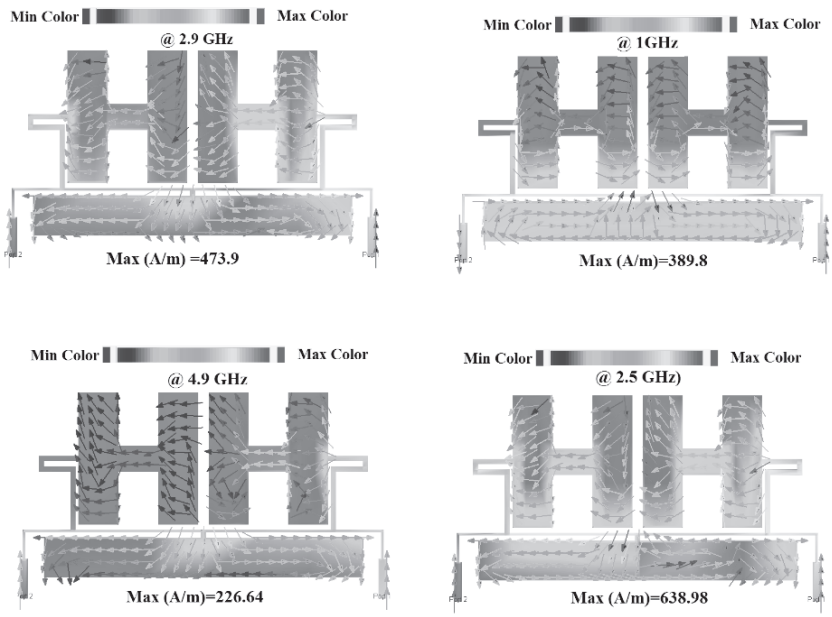

Fig. 5. Current density distribution of the realized filter at 1, 2.5, 2.9 and 4.9 GHz.

Simulation and Measurement Results

The introduced filter is simulated by Advanced Design System (ADS) Momentum Simulator. It is fabricated on a RT_Duroid5880 substrate with a dielectric constant of ε_r=2.2, loss tangent=0.0009 and h=31 mil. An Agilent network analyser N5230A performed the measurements. The simulated and measured S-parameters and a photograph of the fabricated structure are shown in Figure 6. It is clear that the simulation and measurement results are in good agreement. The dashed and solid lines are the measurement and simulation results, respectively. As shown in Figure 6, the measured and simulated harmonics are attenuated up to 11 GHz but there is a harmonic near 12 GHz. The frequency response shows that there is a transmission zero of -50 dB at the stopband.

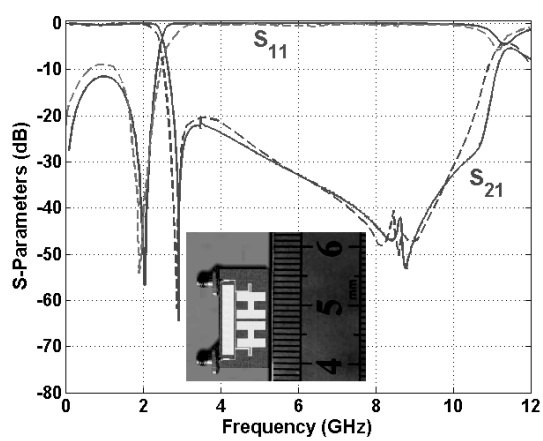

Fig. 6. Simulated and measured S-parameters and a photograph of the fabricated LPF.

According to the obtained results, the proposed LPF has a cut-off frequency of 2.5 GHz, transition band of 0.25 GHz from -3 dB to -20 dB and stop band from 2.79 to 10.9 GHz with a minimum of -20 dB attenuation level. Therefore, the realized filter suppresses the fourth harmonic. Moreover, the overall circuit size is only 0.154 $\lambda_g \times 0.087\ \lambda_g$ (13.8 × 7.8 mm^2), where λ_g is the guided wavelength calculated at 2.5 GHz. The insertion loss and return loss are better than -0.3 dB and -11.47 dB at all passbands. The performance of the proposed LPF is compared to the previous works in Table 4, where Fc and IL are the cut-off frequency and insertion loss, respectively. According to the comparison Table, our designed filter has a good FOM of 10247. According to the comparison results listed in Table 4, only Velidi and Sanyal (2011) could obtain higher FOM than this work. However, the LPF presented in this work has lower insertion loss. Furthermore, our proposed LPF occupies less area so that it is 39% smaller than the LPF designed by Velidi and Sanyal (2011). Only the filter presented by Majidifar (2016) is smaller than that of our work. Nevertheless, our LPF is planar while the LPF proposed by Majidifar (2016) is three-dimensional. On the other hand, Mirzaee and Virdee (2013) and Majidifar (2016) could improve the insertion loss better than us while they have lower figure of merit. Meanwhile, we could reduce the filter size more than 40% in comparison with the LPF proposed by Mirzaee and Virdee (2013).

Table 4. Comparison results (* means approximated values).

References	Fc (GHz)	RSB	SF (dB/10)	ξ (dB/GHz)	NCS (mm^2/λg^2)	AF	FOM	IL (dB)
Majidifar, 2016	1.53	1.53	2.4	29.3	0.0075	2	7172	0.1
Hayati and Lotfi, 2010	1.78	1.4	1	118	0.0425	1	3883	0.3
Verma et al., 2013	2.5	1.14*	2	113.3	0.107	1	2431*	0.72
Chen et al., 2007	2.3	1.56	2.7	188.9	0.207	2	1921	0.5
Yang et al., 2012	3.7	0.63	2	85	0.0514	2	1041	0.5
Karthikeyan and Kshetrimayum, 2015	1.09	1.49	2	48.57	0.0128	2	5690	0.25
Mirzaee and Virdee, 2013	3	1.43	2.5	58.6	0.0242	1	8657	0.03
Sariri et al., 2013	3.9	1.37	2	45.95	0.031	1	4071	0.5
Li and Li, 2008	1.82	1.078	2	40.7	0.0203	1	4312	0.5
Verma and Kumar, 2011	2.5	1.3	2	32	0.243*	2	171*	0.92
Velidi and Sanyal, 2011	0.53	1.4	2	95	0.0222	1	11981	0.5
This work	2.5	1.18	2	58.62	0.0135	1	10247	0.32

CONCLUSION

A compact lowpass filter is presented in this paper, which is designed using a novel symmetrical structure. It consists of the high impedance and rectangular stubs. The layout structure was analysed using an LC model so that the simulation results of LC circuit were similar to the EM simulator results of layout configuration. This means that the lumped capacitors and inductors are calculated correctly. A comparison between our filter and previous works was carried out that verified its high performance. In addition, a compact size was obtained by our novel structure. Meanwhile, a low insertion loss of 0.3 dB was obtained, which is good in comparison with the previous works. According to the comparison table, the proposed Lowpass filter has a good figure of merit, which shows a high performance. Moreover, to confirm the calculated data from LC model and EM simulator results, the realized LPF was fabricated and measured.

REFERENCES

Chen, J., Weng, Z.-B., Jiao, Y.-C. & Zhang, F.-S. 2007. Lowpass Filter Design of Hilbert Curve Ring Defected Ground Structure. Progress in Electromagnetics Research 70: 269–280.

Deng, P.-H., Huang, B.-L. & Chen, B.-L. 2015. Designs of Microstrip Four- and Five-Channel Multiplexers Using Branch-Line-Shaped Matching Circuits. IEEE Transaction on Components Packing and Manufacturing Technology. **5**(9): 1331–1338.

Ghazali, A.N., Sazid, M. & Pal, S. 2018. Dual band notched UWB-BPF based on hybrid microstrip-to-CPW transition. AEU - International Journal of Electronics and Communications 86: 55–62.

Hayati M. & Lotfi, A. 2010. Elliptic-function lowpass filter with sharp cutoff frequency using slit-loaded tapered compact microstrip resonator cell. Electronics Letters **46**(2):143–144.

Hong, J.S. & Lancaster, M.J. 2001. Microstrip Filters for RF/Microwave Applications. John Wiley & Sons.

Karpuz, C., Gorur, A.K. & Emur, M. 2016. Quad-Band Microstrip Bandstop Filter Design Using Dual-Mode Open Loop Resonators Having Thin Film Capacitors. IEEE Microwave and Wireless Components Letters **26**(11): 873–875.

Karthikeyan, S.S. & Kshetrimayum, R.S. 2015. Compact and Wide Stopband Lowpass Filter Using Open Complementary Split Ring Resonator and Defected Ground Structure. Radioengineering **24**(3): 708–711.

Li, L. & Li, Z.-F. 2008. Compact quasi-elliptic lowpass filter using symmetric rectangular coupled capacitors. Electronics Letters **44**(2): 124–125.

Li, Q. & Zhang, Y. 2017. Six-channel diplexer with compact size and high isolation. Electronics Letters **53**(17): 1205–1207.

Majidifar, S. 2016. Design of High Performance Miniaturized Lowpass Filter Using New Approach of Modeling. Applied Computational Electromagnetics Society Journal **31**(1): 52–57.

Mirzaee, M. & Virdee, B.S. 2013. Realizations of highly compact planar lowpass filter for UWB RFID applications. Electronics Letters **49** (22): 1396–1398.

Rezaei, A., Noori, L. & Mohammadi, H. 2017. Design of a novel compact microstrip diplexer with low insertion loss. Microwave and optical Technology Letters **59**(7):1672–1676.

Sariri, H., Rahmani, Z., Lalbakhsh, A. & Majidifar, S. 2013. Compact LPF Using T-shaped Resonator. Frequenz Journal **67**(1–2): 17–20.

Sohn, S.-M., Gopinath A. & Vaughan, J.-T. 2016. A Compact, High Power Capable, and Tunable High Directivity Microstrip Coupler. IEEE Transactions on Microwave Theory and Techniques **64**(10): 3217–3223

Velidi, V.K. & Sanyal, S. 2011. Sharp Roll-Off Lowpass Filter with Wide Stopband Using Stub-Loaded Coupled-Line Hairpin Unit. IEEE Microwave and Wireless Components Letters **21**(6): 301–303.

Verma, A.K., Chaudhari, N.P. & Kumar, A. 2013. Improved performance step impedance lowpass filter. International Journal of Electronics and Communications (AEÜ) **67**(9): 761–770.

Verma, A.K. & Kumar, A. 2011. Design of low-pass filters using some defected ground structures. International Journal of Electronics and Communications (AEÜ). **65**(10) 864–872.

Wang, L., Wang, G. & Siden, J. 2017. High-performance tight coupling microstrip directional coupler with fragment-type compensated structure. IET Microwaves, Antennas & Propagation **11**(7): 1057–1063

Wadell, Brian C. 1991. Transmission Line Design Handbook. Artech House.

Yang, Y., Zhu, X. & Karmakar, N.C. 2012. Microstrip Lowpass Filter Based on Split Ring and Complementary Split Ring Resonators. Microwave and optical Technology Letters **54**(7): 1723–1726.

SUBMITTED: 24/05/2017
REVISED : 14/12/2017
ACCEPTED : 27/03/2018

تصميم جديد لمرشح الترددات المنخفضة المسطح باستخدام شريحة شريطية مستطيلة الشكل وخلايا ذات مقاومة عالية في أنظمة الاتصالات اللاسلكية

عباس رضايي* و ليلا نوري**

* قسم هندسة الكهرباء، جامعة كرمانشاه الصناعية، كرمانشاه، الجمهورية الإسلامية الإيرانية.
** منتدى الباحثين الشباب، فرع كرمانشاه، جامعة آزاد الإسلامية، كرمانشاه ، الجمهورية الإسلامية الإيرانية.

الخلاصة

يقدم هذا البحث مرشح جديد ذو ترددات منخفضة شريطي. يتكون المرشح المقترح من خليتين عاليتي المقاومة، تم دمجهما بواسطة خط إرسال مُحَمل. يتم استخدام كعب مستطيل لتقليل حجم الدائرة الكلي بحيث يكون حجمه المضغوط هو $0.0135\ \lambda g^2$ حيث أن λg هو الطول الموجي المحسوب عند 2.5 GHz. وبالمقارنة مع الأبحاث السابقة، تم الحصول على معامل استحقاق جيد (FOM) يشير إلى أنه تم تصميم هذا المرشح بشكل صحيح. تم إدخال دائرة مستحث ومكثفLC لتحليل صورة الهيكل المقترح. وبناءً على نظرية خط النقل، تم حساب العناصر المُجمعة. وبعد ذلك، تم محاكاة نموذج LC حيث كانت النتائج التي تم الحصول عليها مشابهة لنتائج محاكاة EM. ومن أجل التأكد من منهجية التصميم، تم تصنيع وقياس الفلتر المقترح، وكان هناك توافق جيد بين نتائج المحاكاة والقياس.